

Statistical Neurodynamics of Deep Networks: Geometry of Signal Spaces

Shun-ichi Amari^{*†} Ryo Karakida[†] Masafumi Oizumi[‡]

Abstract

Statistical neurodynamics studies macroscopic behaviors of randomly connected neural networks. We consider a deep layered feedforward network where input signals are processed layer by layer. The manifold of input signals is embedded in a higher dimensional manifold of the next layer as a curved submanifold, provided the number of neurons is larger than that of inputs. We show geometrical features of the embedded manifold, proving that the manifold enlarges or shrinks locally isotropically so that it is always embedded conformally. We study the curvature of the embedded manifold. The scalar curvature converges to a constant or diverges to infinity slowly. The distance between two signals also changes, converging eventually to a stable fixed value, provided both the number of neurons in a layer and the number of layers tend to infinity. This causes a problem, since when we consider a curve in the input space, it is mapped as a continuous curve of fractal nature, but our theory contradictorily suggests that the curve eventually converges to a discrete set of equally spaced points. In reality, the numbers of neurons and layers are finite and thus, it is expected that the finite size effect causes the discrepancies between our theory and reality. We need to further study the discrepancies to understand their implications on information processing.

^{*}RIKEN CBS, Wako-shi, Japan

[†]AIST, Tokyo, Japan

[‡]Araya Co., Tokyo, Japan

1 Introduction

Statistical dynamics bases studies of the behaviors of macroscopic quantities such as temperature and entropy, on the microscopic physical laws of molecular particles, by using the statistical averages of random variables. Statistical neurodynamics infers the macroscopic behaviors of randomly connected neural networks from the microscopic signal processing of component neurons. This idea originated from the work of Rozonoer (1969) and Amari (1970, 1971), and its mathematical foundation was further studied by Amari (1974) and Amari et al. (1977).

Poole et al. (2016) used the method of statistical neurodynamics to elucidate the behaviors of randomly connected deep feedforward neural networks, giving a new perspective to examine deep networks, and Schoenholz et al. (2016) applied it to backpropagation learning in deep networks. Inspired by these studies, the present paper investigates how geometrical structures of signal spaces develop layer by layer (See also our accompanying paper (Amari, Karakida & Oizumi, 2018) for the analysis of the Fisher information and natural gradient).

An input space is embedded in the output space of a layer when the number of neurons is larger than the number of inputs. The embedded manifold is curved and enlarges or shrinks, eventually giving rise to a fractal structure. The metric of a signal space develops conformally so that the tangent spaces are rotated with isotropical enlargement or shrinkage. We study the metric and curvature based on the mean field approximation.

There are three main findings in the present paper. First, we show that the metric tensor is conformally changed through layers. Second, we explicitly calculate how the curvature (extrinsic curvature tensor and affine connection of the embedded manifold) changes through layers. It converges to a fixed value under a certain condition (chaotic regime of Poole et al., 2016) and diverges very slowly under the other condition. Third, we elucidate the distance law, which describes how the distance between two signal points changes through layers. We demonstrate that there is a contradiction between the real situation where both the number of layers and the number of neurons are finite and the ideal theoretical situation where both tend to infinity, as described below.

The distance between two signals changes as signals are processed in layers and its dynamics

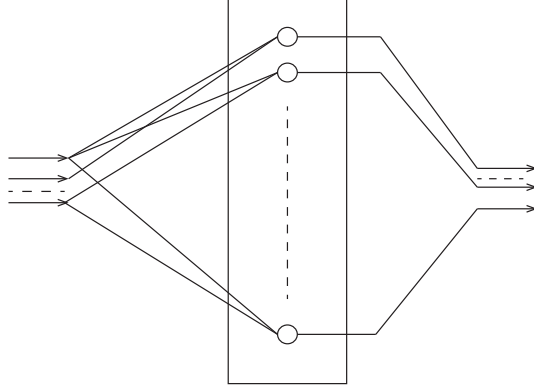


Figure 1: Input-output relation of a layer

has a stable equilibrium point. Such a dynamics of distance was proposed in Amari (1974) and Amari et al. (1977) and applied to randomly connected recurrent networks to study microscopic characteristics of their attractors (Amari et al. 2013; Toyozumi et al. 2015). Poole et al. (2016) expressed the distance law for deep layered feedforward networks in terms of the overlap of two inputs, which is equivalent to the distance between them. However, the dynamic law of distance is problematic because the distance between any two signals eventually converges to a constant in the limit when the number of neurons in each layer is infinitely large and the number of layers is also infinitely large.

Let us consider a curve $\mathbf{x}(s)$ in the input space, where s is the parameter describing the curve. It is embedded in a higher dimensional manifold continuously, so it is impossible that the curve converges to a set of equally spaced points in the case that both the numbers of neurons and the number layers are finite. The curve has a fractal structure and frustrations take place between continuity and discreteness. We will finally remark the importance of the effect of the finiteness of the numbers of neurons and layers.

2 Layered feed-forward network of random connections

Let us consider a feed-forward network consisting of m neurons that receive n -dimensional inputs $\mathbf{x} = (x_1, \dots, x_n)$ (see Figure 1). Let $\mathbf{y} = (y_1, \dots, y_m)$ be the outputs from the m neurons. Let $w_{i\kappa}$ be the connection weight from the κ -th input to neuron i and b_i be the

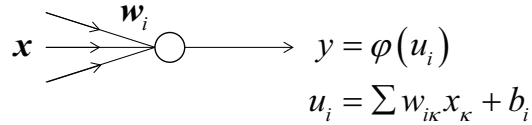


Figure 2: Input-output relation of neuron i

bias term of neuron i . We use indices κ, λ, \dots for input vectors and indices i, j, \dots for output vectors. The sum of stimuli for neuron i is

$$u_i = \sum_{\kappa} w_{i\kappa} x_{\kappa} + b_i \quad (1)$$

and the output from that neuron is

$$y_i = \varphi(u_i), \quad (2)$$

where φ is an output function (see Figure 2). We use the error function

$$\varphi(u) = \frac{1}{\sqrt{2\pi}} \int_{-\infty}^u \exp\left\{-\frac{v^2}{2}\right\} dv, \quad (3)$$

because this is convenient for obtaining analytical formulas. The behaviors of the network are qualitatively the same if other output functions are used.

We assume that the connection weights $w_{i\kappa}$ and the bias b_i are independent random variables having Gaussian distributions with variances σ^2/n and σ_b^2 , respectively, and mean 0. Then, all u_i are independent random variables subject to the same Gaussian distribution with mean 0 and variance

$$\tau^2 = \frac{\sigma^2}{n} \sum x_{\kappa}^2 + \sigma_b^2. \quad (4)$$

The outputs $y_i = \varphi(u_i)$ are nonlinear functions of u_i , so they are also independently and identically distributed.

We consider a deep network consisting of concatenated feedforward layers. The t -th layer receives input \mathbf{x}^{t-1} which is the output of the previous layer $t-1$ and emits output \mathbf{x}^t (see Figure 3). The connection weights and biases are w_{ij}^t and b_i^t , subject to the same 0 mean independent Gaussian distributions with variance σ_t^2/n_{t-1} , and σ_b^2 , respectively, where n^t is

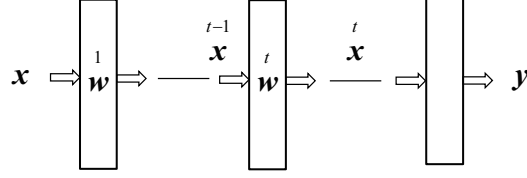


Figure 3: Deep layered network

the number of neurons in layer t . The output is written as

$$x_i^t = \varphi(u_i^t), \quad (5)$$

$$u_i^t = \sum w_{ij}^t x_j^{t-1} + b_i^t \quad (6)$$

or, in the vector-matrix notation,

$$\mathbf{x}^t = \varphi(\mathbf{W}^t \mathbf{x}^{t-1} + \mathbf{b}^t). \quad (7)$$

Let X^{t-1} be the input signal space consisting of n^{t-1} -dimensional input signals \mathbf{x}^{t-1} and X^t be the n^t -dimensional output signal space of layer t . When $n^t \geq n^{t-1}$, the manifold X^{t-1} is embedded in X^t . When $n^t < n^{t-1}$, X^{t-1} is mapped to a lower-dimensional X^t by a many-to-one mapping.

Since the original input manifold $X = X^0$ is transformed layer by layer successively, its image at layer t is denoted by \tilde{X}^t which is a submanifold embedded in X^t . We infer the geometry of \tilde{X}^t from that of \tilde{X}^{t-1} .

3 Propagation of activities

We consider as a simple macroscopic quantity the activity of output \mathbf{x}^t of layer t defined by

$$A^t = \frac{1}{n^t} \sum (x_i^t)^2. \quad (8)$$

This is written as

$$A^t = \frac{1}{n^t} \sum \{\varphi(u_i^t)\}^2. \quad (9)$$

Since u_i^t are independent random Gaussian variables with mean 0 and variance

$$\tau_t^2 = \sigma_t^2 A^{t-1} + \sigma_b^2, \quad (10)$$

the law of large numbers guarantees that it converges to the expectation

$$A^t = \mathbb{E} \left[\{\varphi(u_i^t)\}^2 \right], \quad (11)$$

when n^t is sufficiently large, where \mathbb{E} denotes the expectation with respect to w_{ij}^t and b_i^t .

In order to calculate the expectations of various quantities like A^t , we define a fundamental function χ_0 by

$$\chi_0(\sigma^2, A) = \int \varphi^2(\sigma_A v) Dv, \quad (12)$$

where $\sigma_A^2 = \sigma^2 A + \sigma_b^2$ and

$$Dv = \frac{1}{\sqrt{2\pi}} \exp\left\{-\frac{v^2}{2}\right\} dv. \quad (13)$$

For later use, we define the p -th fundamental functions χ_p ($p = 1, 2$) by

$$\chi_1(\sigma^2, A) = \sigma^2 \int \{\varphi'(\sigma_A v)\}^2 Dv, \quad (14)$$

$$\chi_2(\sigma^2, A) = \sigma^4 \int \{\varphi''(\sigma_A v)\}^2 Dv. \quad (15)$$

Since u_i^t is subject to $N(0, \tau_t^2)$, we have

$$\mathbb{E} \left[\{\varphi(u_i^t)\}^2 \right] = \frac{1}{\sqrt{2\pi\tau_t}} \int \{\varphi(u)\}^2 \exp\left\{-\frac{u^2}{2\tau_t^2}\right\} du \quad (16)$$

$$= \chi_0(\sigma_t^2, A^{t-1}). \quad (17)$$

When φ is the error function,

$$\chi_0(\sigma^2, A) = \frac{1}{2\pi} \cos^{-1} \left(\frac{-\sigma_A^2}{1 + \sigma_A^2} \right), \quad (18)$$

as is seen in Appendix I. Hence we have the following theorem, describing how the activity develops.

Theorem 1. The activity develops as

$$A^t = \chi_0(\sigma_t^2, A^{t-1}). \quad (19)$$

Since $\chi_0(\sigma^2, A)$ is a monotonically increasing function of A , when $\sigma_t^2 = \sigma^2$ for all t , there is an equilibrium \bar{A} satisfying

$$\chi_0(\sigma^2, \bar{A}) = \bar{A}, \quad (20)$$

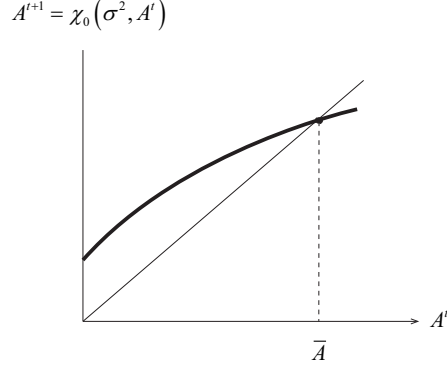


Figure 4: Dynamics of A^t and its equilibrium \bar{A}

that is uniquely determined and is stable (see Figure 4). In this case, as t becomes large, A^t converges to \bar{A} quickly. Hence \tilde{X}^t is concentrated on the sphere of radius \bar{A} in X^t

$$\frac{1}{n_t} \sum (x_i^t)^2 = \bar{A}, \quad (21)$$

with small fluctuations in the radius directions. When σ_t^2 are different, however, the radius A^t of the sphere fluctuates.

4 Development of metric

We consider again layer t , in which inputs are \mathbf{x}^{t-1} belonging to \tilde{X}^{t-1} and the outputs $\tilde{\mathbf{x}}^t$ constitute \tilde{X}^t . This section treats the case of $n^t \geq n^{t-1}$ for all t , so n_0 -dimensional \tilde{X}^{t-1} is embedded in an n_t -dimensional manifold X^t . The image $\tilde{X}^t \subset X^t$ is a curved n_0 -dimensional manifold, provided $n^t \geq n^{t-1} \dots \geq n^0 = n$.

We first consider the input signal space $X = X^0$, which is assumed to be a Euclidean space. Let $\{\mathbf{e}_\kappa\}$ be the set of orthonormal basis vectors in the input manifold X along the coordinate axis x_κ . So the small line element $d\mathbf{x}$ connecting \mathbf{x} and $\mathbf{x} + d\mathbf{x}$ is written as

$$d\mathbf{x} = \sum dx_\kappa \mathbf{e}_\kappa. \quad (22)$$

We consider the output signal submanifold \tilde{X}^t of layer t . Coordinate lines x_κ in input X become curved lines \tilde{x}_κ^t in \tilde{X}^t and let $\{\tilde{\mathbf{e}}_\kappa^t\}$ be the basis vectors in the tangent space of \tilde{X}^t along the coordinate curves x_κ . See Fig. 5.

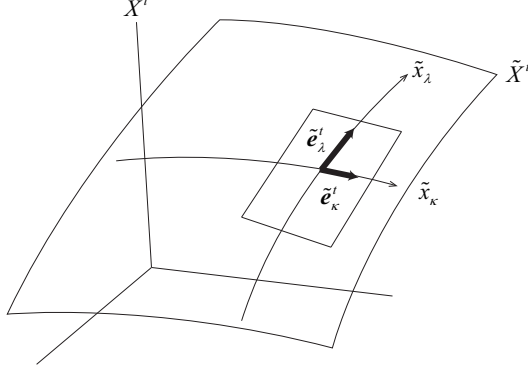


Figure 5: Tangent Space of \tilde{X}^t and basis vectors

A small line element $d\tilde{\mathbf{x}}^{t-1}$ in \tilde{X}^{t-1} changes to $d\tilde{\mathbf{x}}^t$ as

$$d\tilde{x}_i^t = \sum B_{ij}^t d\tilde{x}_j^{t-1}, \quad (23)$$

where the Jacobian matrix $\mathbf{B}^t = (B_{ij}^t)$ of (7) is,

$$B_{ij}^t = \frac{\partial \tilde{x}_i^t}{\partial \tilde{x}_j^{t-1}} = \frac{\partial \varphi(u_i^t)}{\partial \tilde{x}_j^{t-1}}. \quad (24)$$

Both $d\tilde{\mathbf{x}}^t$ and $d\tilde{\mathbf{x}}^{t-1}$ belong to the tangent spaces of \tilde{X}_t and \tilde{X}_{t-1} , respectively. The basis vector $\tilde{\mathbf{e}}_\kappa^t$ of the tangent space of \tilde{X}^t is a vector in X^t ,

$$\tilde{\mathbf{e}}_\kappa^t = \frac{\partial \tilde{\mathbf{x}}^t}{\partial x_\kappa}, \quad (25)$$

the i -th component of which is

$$(\tilde{\mathbf{e}}_\kappa^t)_i = \frac{\partial \tilde{x}_i^t}{\partial x_\kappa}. \quad i = 1, \dots, n_t. \quad (26)$$

We see that $\tilde{\mathbf{e}}_\kappa^{t-1} = (e_{\kappa j}^{t-1})$ is mapped to $\tilde{\mathbf{e}}_\kappa^t = (e_{\kappa i}^t)$ linearly as

$$e_{\kappa i}^t = \sum_j B_{ij}^t e_{\kappa j}^{t-1}. \quad (27)$$

We introduce a metric tensor to the input signal manifold X by using the basis vectors of the t -th layer given by

$$g_{\kappa\lambda}^t = \langle \tilde{\mathbf{e}}_\kappa^t, \tilde{\mathbf{e}}_\lambda^t \rangle = \sum e_{\kappa i}^t e_{\lambda i}^t, \quad (28)$$

where \langle , \rangle is the inner product in the Euclidean space X^t . This is a Riemannian metric of X pulled-back from \tilde{X}^t to X . The new squared length of $d\mathbf{x}$ in the input space X due to the

induced metric $g_{\kappa\lambda}^t$ is

$$(ds^2)^t = \sum g_{\kappa\lambda}^t dx_\kappa dx_\lambda, \quad (29)$$

which is given by the squared Euclidean length of $d\tilde{\mathbf{x}}^t$ of layer t .

From (27), we have

$$\langle \tilde{\mathbf{e}}_\kappa^t, \tilde{\mathbf{e}}_\lambda^t \rangle = \sum_{i,j,k,l} B_{ik}^t B_{jl}^t \delta_{ij} e_{\kappa l}^{t-1} e_{\lambda k}^{t-1}, \quad (30)$$

where δ_{ij} is the Kronecker delta. When n_t is sufficiently large, by the law of large numbers,

$$\frac{1}{n_t} \sum_i B_{ik}^t B_{il}^t = \mathbb{E} \left[\{\varphi'(u_i^t)\}^2 w_{ik}^t w_{il}^t \right]. \quad (31)$$

If the two terms in the expectation (31) split as

$$\mathbb{E} \left[\{\varphi'(u_i^t)\}^2 w_{ij}^t w_{ik}^t \right] = \mathbb{E} \left[\{\varphi'(u_i^t)\}^2 \right] \mathbb{E} [w_{ij}^t w_{ik}^t], \quad (32)$$

the respective expectations are calculated from

$$\chi_{1,t}(\sigma_t^2, A^{t-1}) = \sigma_t^2 \mathbb{E} \left[\{\varphi'(u_i^t)\}^2 \right], \quad (33)$$

$$\mathbb{E} [w_{ik}^t w_{il}^t] = \frac{\sigma_t^2}{n_t} \delta_{kl}. \quad (34)$$

The split lemma given in Appendix II guarantees (32) holds when n_t is sufficiently large.

Theorem 2. The metric is transformed as

$$g_{\kappa\lambda}^t(\mathbf{x}) = \chi_{1,t}(\mathbf{x}) g_{\kappa\lambda}^{t-1}(\mathbf{x}). \quad (35)$$

Proof. From (28) by using (30)–(34) and

$$\sum \delta_{kl} e_{\kappa k}^{t-1} e_{\lambda l}^{t-1} = \langle \tilde{\mathbf{e}}_\kappa^{t-1}, \tilde{\mathbf{e}}_\lambda^{t-1} \rangle = g_{\kappa\lambda}^{t-1}, \quad (36)$$

we have the theorem.

When a metric tensor is transformed in the following form

$$\tilde{g}_{\kappa\lambda}(\mathbf{x}) = \rho(\mathbf{x}) g_{\kappa\lambda}(\mathbf{x}) \quad (37)$$

for a scalar function $\rho(\mathbf{x})$, the transformation is conformal. A conformal transformation does not alter the angle of two tangent vectors, so two orthogonal line elements are always orthogonal after the transformation. This implies that the tangent space is subject to two kinds of transformation without changing the shape:

- 1) isotropic enlargement/shrinkage;
- 2) rotation.

From (35), the metric induced from layer t is obtained as

$$g_{\kappa\lambda}^t(\mathbf{x}) = \chi_t^*(\mathbf{x})\delta_{\kappa\lambda}, \quad (38)$$

where we put

$$\chi_t^* = \prod_{s=1}^{t-1} \chi_{1,s}. \quad (39)$$

When $\sigma_t^2 = \sigma^2$ and t is large, A^t converges to \bar{A} . Hence, we have asymptotically a simple form of metric

$$g_{\kappa\lambda}^t(\mathbf{x}) \approx \{\bar{\chi}_1\}^{t-1} \delta_{\kappa\lambda}, \quad (40)$$

$$\bar{\chi}_1 = \chi_1(\sigma^2, \bar{A}), \quad (41)$$

except for fluctuating terms of order $1/\sqrt{n}$. When φ is the error function, we have

$$\chi_1(\sigma^2, A) = \frac{\sigma^2}{2\pi} \frac{\sigma_b^2 + \sigma^2 A}{\sqrt{1 + 2(\sigma_b^2 + \sigma^2 A)}} \quad (42)$$

(see Appendix I).

When $\bar{\chi}_1 < 1$, $g_{\kappa\lambda}^t$ converges to 0 because of (39), implying that $d\tilde{\mathbf{x}}^t$ shrinks to 0. Hence no interesting information processing takes place. This happens when both σ^2 and σ_b^2 are small enough. When they are large enough, $\bar{\chi} > 1$, and the length of a line element becomes infinitely large as t becomes large. However, the signals lie in a bounded region of X^t because of $|x_i| \leq 1$ except in the case of a ReLU activation function. Therefore, if we consider a curve $\mathbf{x}(s)$ in the input space, its image must be highly curved like a Peano curve, because the length of two adjacent points is always enlarged (Poole et al., 2016). This suggests a chaotic dynamics for \mathbf{x}^t . Such phenomena are possible when the image \tilde{X}^t of X becomes highly curved in X^t .

We next study the curvature of \tilde{X}^t . When σ_t^2 are designed such that $\chi_t^* \approx 1$, g_{ij}^t neither diverges nor converges to 0. So \tilde{X}^t is deformed with slight expansion or shrinkage but with high curvature. Interesting information processing takes place at such an edge of chaos (Yang & Schoenholz, 2018).

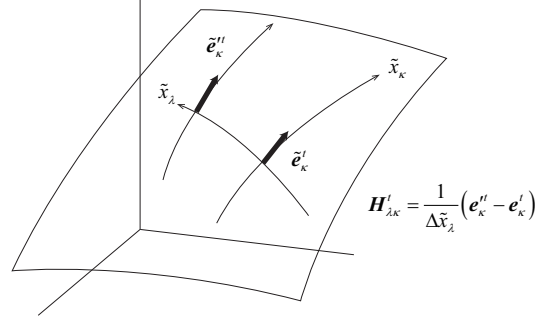


Figure 6: Curvature and affine connections: How $\tilde{\mathbf{e}}_\kappa^t$ changes along the \tilde{x}_λ^t axis.

5 Curvatures of signal manifolds

The curvature of the embedded manifold \tilde{X}^t is measured by the quantities showing how the basis vectors $\tilde{\mathbf{e}}_\kappa^t$ of the tangent space of \tilde{X}^t change as the point $\tilde{\mathbf{x}}^t$ moves in the direction of $\tilde{\mathbf{e}}_\lambda^t$. (see Figure 6). By using the directional derivative ∇_λ , they are given by the vector

$$\mathbf{H}_{\kappa\lambda}^t = \nabla_\lambda \tilde{\mathbf{e}}_\kappa^t, \quad (43)$$

where ∇_λ is the covariant derivative in the ambient manifold X^t . However, X^t is a Euclidean space, so ∇_λ is the partial derivative with respect to \tilde{x}_λ that is $\nabla_\lambda = \partial/\partial x_\lambda$. $\mathbf{H}_{\kappa\lambda}^t$ is a vector in X^t for fixed indices κ and λ and is a tensor in X having two indices κ and λ .

We can decompose $\mathbf{H}_{\kappa\lambda}^t$ as a sum of a vector orthogonal to the tangent space of $\tilde{X}^t \subset X^t$ and a vector in the tangent space. The orthogonal one shows how \tilde{X}^t is curved in the orthogonal direction of \tilde{X}^t , whereas the tangential vector demonstrates deformations of $\{\tilde{\mathbf{e}}_\kappa^t\}$ inside \tilde{X}^t . Mathematically, the former is the embedding, extrinsic or Euler-Schouten curvature, showing how \tilde{X}^t is curved in X^t . The latter represents components of the affine connection that shows how the coordinate system \tilde{x}_κ^t is curved inside the manifold \tilde{X}^t . For the moment, we do not decompose $\mathbf{H}_{\kappa\lambda}^t$ and simply call it the curvature vector.

The curvature vectors are given in the component form by

$$H_{\kappa\lambda i}^t = \partial_\lambda \partial_\kappa \varphi(u_i^t) = \partial_\lambda e_{\kappa i}^t, \quad (44)$$

where

$$\partial_\kappa = \frac{\partial}{\partial x_\kappa}. \quad (45)$$

We further have, from (27),

$$H_{\kappa\lambda i}^t = \partial_\kappa \left\{ \sum \varphi'(u_i) w_{ij} \partial_\lambda \tilde{x}_j^{t-1} \right\} \quad (46)$$

$$= \varphi''(u_i) (\mathbf{w}_i \cdot \partial_\kappa \tilde{\mathbf{x}}^{t-1}) (\mathbf{w}_i \cdot \partial_\lambda \tilde{\mathbf{x}}^{t-1}) \quad (47)$$

$$+ \varphi'(u_i) \mathbf{w}_i \cdot \partial_\kappa \partial_\lambda \tilde{\mathbf{x}}^{t-1}, \quad (48)$$

where $\mathbf{w}_i = (w_{ij}^t)$ and we omit the superscript t attached to w_{ij} and u_i . By noting

$$\mathbf{H}_{\kappa\lambda}^{t-1} = \partial_\kappa \partial_\lambda \tilde{\mathbf{x}}^{t-1}, \quad (49)$$

the following recursive equation is obtained

$$H_{\kappa\lambda i}^t = \varphi''(u_i) (\mathbf{w}_i \cdot \tilde{\mathbf{e}}_\kappa^{t-1}) (\mathbf{w}_i \cdot \tilde{\mathbf{e}}_\lambda^{t-1}) + \varphi'(u_i) \mathbf{w}_i \cdot \mathbf{H}_{\kappa\lambda}^{t-1}. \quad (50)$$

We define the magnitude of the curvature vector by

$$|\mathbf{H}_{\kappa\lambda}^t|^2 = \langle \mathbf{H}_{\kappa\lambda}^t, \mathbf{H}_{\kappa\lambda}^t \rangle = \sum_i (H_{\kappa\lambda i}^t)^2 \quad (51)$$

and replace the summation by the expectation by using the law of large numbers. Then, we have

$$|\mathbf{H}_{\kappa\lambda}^t|^2 = n_t \mathbb{E} \left[\{ \varphi''(u_i) \}^2 (\mathbf{w} \cdot \tilde{\mathbf{e}}_\kappa^{t-1})^2 (\mathbf{w} \cdot \tilde{\mathbf{e}}_\lambda^{t-1})^2 \right] \quad (52)$$

$$+ 2n_t \mathbb{E} \left[\varphi'(u_i) \varphi''(u_i) (\mathbf{w} \cdot \tilde{\mathbf{e}}_\kappa^{t-1}) (\mathbf{w} \cdot \tilde{\mathbf{e}}_\lambda^{t-1}) (\mathbf{w} \cdot \partial_\kappa \tilde{\mathbf{e}}_\lambda^{t-1}) \right] \quad (53)$$

$$+ n_t \mathbb{E} \left[\{ \varphi'(u_i) \}^2 (\mathbf{w} \cdot \mathbf{H}_{\kappa\lambda}^{t-1})^2 \right]. \quad (54)$$

It consists of three terms. The second term vanishes because it is an odd function of \mathbf{w} . We use the split lemma given Appendix II that the terms of functions of u_i and the remaining terms (the second or fourth order terms of \mathbf{w}) split in the expectation. This is because the terms $\varphi'(u_i)$ and $\varphi''(u_i)$ have the self-averaging property (the mean field approximation).

The first term is the product of

$$\mathbb{E} \left[\{ \varphi''(u_i) \}^2 \right] = \frac{1}{\sigma_t^4} \chi_2(\sigma_t^2, A^{t-1}) \quad (55)$$

and

$$\mathbb{E} \left[(\mathbf{w} \cdot \tilde{\mathbf{e}}_\kappa^{t-1})^2 (\mathbf{w} \cdot \tilde{\mathbf{e}}_\lambda^{t-1})^2 \right] = \frac{\sigma_t^4}{n_t^2} (1 + 2\delta_{\kappa\lambda}) |\tilde{\mathbf{e}}_\kappa^{t-1}|^2 |\tilde{\mathbf{e}}_\lambda^{t-1}|^2, \quad (56)$$

where we use

$$E [w_i w_j w_k w_l] = \frac{\sigma_t^4}{n_t^2} (\delta_{ij} \delta_{kl} + \delta_{ik} \delta_{jl} + \delta_{il} \delta_{jk}). \quad (57)$$

The third term is

$$E [\varphi'^2] E \left[(\mathbf{w} \cdot \mathbf{H}_{\kappa\lambda}^{t-1})^2 \right] = \chi_1 (\sigma_t^2, A^{t-1}) |\mathbf{H}_{\kappa\lambda}^{t-1}|^2. \quad (58)$$

Therefore, we have

$$|\mathbf{H}_{\kappa\lambda}^t|^2 = \chi_1 (\sigma_t^2, A^{t-1}) |\mathbf{H}_{\kappa\lambda}^{t-1}|^2 + \frac{1}{n_t} (1 + 2\delta_{\kappa\lambda}) \{ \chi_2 (\sigma_t^2, A^{t-1}) \} (g_{\kappa\kappa}^{t-1})^2 (g_{\lambda\lambda}^{t-1})^2. \quad (59)$$

We did not distinguish the embedding curvature and affine connection. Since \mathbf{w}_i is isotropically distributed in X^t , when n_t^\perp is the number of dimensions orthogonal to \tilde{X}^t , (n_t^\perp/n_t) $|\mathbf{H}_{\kappa\lambda}|^2$ is the extrinsic curvature tensor and $(1 - n_t^\perp/n_t)$ $|\mathbf{H}_{\kappa\lambda}|^2$ is due to the affine connection, because of the equipartition property.

We further simplify the situation by defining the scalar curvature

$$\gamma_t^2 = \frac{1}{n_t} \sum (g_t^{-1})^{\kappa\mu} (g_t^{-1})^{\lambda\nu} H_{\kappa\lambda i}^t H_{\mu\nu j}^t \delta_{ij}, \quad (60)$$

where $(g_t^{-1})^{\kappa\lambda}$ is the inverse matrix of $(g_{\kappa\lambda}^t)$.

From

$$(g_t^{-1})^{\kappa\lambda} = \frac{1}{\chi_{1,t-1}} (g_{t-1}^{-1})^{\kappa\lambda} \quad (61)$$

we have the following recursive equation

$$\gamma_t^2 = \frac{\gamma_{t-1}^2}{\chi_{1,t-1}} + 3 \frac{\chi_{2,t-1}}{n_t (\chi_{1,t-1})^2}. \quad (62)$$

The first term on the right-hand side of (62) shows the curvature inherited from the input with decay factor χ_1^{-1} and the second term is the newly created curvature in the layer. This gives

$$\gamma_t^2 = 3 \frac{1}{n_t} \sum_{s=1}^{t-1} \frac{\chi_{2,t-s}}{\chi_{1,t-s}^2} \left(\prod_{r=1}^s \frac{1}{\chi_{1,t-r}} \right). \quad (63)$$

When t is sufficiently large and $\sigma_t^2 = \sigma^2$ and $\chi_1 = \chi_{1,t} > 1$, we have

$$\gamma_t^2 = \frac{3\chi_2}{n_t \chi_1 (\chi_1 - 1)}, \quad (64)$$

implying that the scalar curvature converges to a small constant. This is the result obtained by Poole et al. (2016) when X is a 1-dimensional curve. When $\chi_1 < 1$, γ_t^2 diverges to infinity, provided n_t are finite although they are large, in spite that \tilde{X}^t shrinks.

When $\chi_t^* \approx 1$, which implies the network dynamics is at the edge of chaos (Poole et al. 2016; Schoenholz et al. 2017), the induced metric is

$$g_{\kappa\lambda}^t \approx \delta_{\kappa\lambda}, \quad (65)$$

except for higher-order fluctuations, keeping the length and orthogonality. However, even though new creations of curvature are small (the second terms of (62) is of order $1/n_s$), they accumulate and

$$\gamma_t^2 \approx 3 \sum_{s=1}^{t-1} \frac{1}{n_s} \frac{\chi_{2,s}}{\chi_{1,s}^2} \quad (66)$$

diverges to infinity, provided n_s are finite. Hence, although the metric is well controlled, \tilde{X}^t is highly deformed since the coordinates $\tilde{\mathbf{x}}^t$ are highly distorted in \tilde{X}^t .

6 Law of distance

Let \mathbf{x}^{t-1} and \mathbf{y}^{t-1} be two input signals at layer t . Their outputs are \mathbf{x}^t and \mathbf{y}^t , respectively.

Let

$$D_t = D(\mathbf{x}^t, \mathbf{y}^t) = \frac{1}{n_t} \sum (x_i^t - y_i^t)^2 \quad (67)$$

be the squared Euclidean distance between two signals \mathbf{x}^t and \mathbf{y}^t divided by n_t . We study how D_t is related to D_{t-1} . When \mathbf{x}^{t-1} and \mathbf{y}^{t-1} are infinitesimally close, $d\mathbf{x}^{t-1} = \mathbf{x}^{t-1} - \mathbf{y}^{t-1}$ belongs to the tangent space and it expands or shrinks by a scalar factor χ_1 depending on whether it is larger than 1 or not. Here, we study how the distance develops when \mathbf{y}^{t-1} and \mathbf{x}^{t-1} are not necessarily close.

It is easier to study how the overlap

$$C_t = C(\mathbf{x}, \mathbf{y}) = \frac{1}{n_t \sqrt{A(\mathbf{x}^t) A(\mathbf{y}^t)}} \sum x_i^t y_i^t \quad (68)$$

develops. The distance and overlap are related by

$$D(\mathbf{x}, \mathbf{y}) = A(\mathbf{x}) + A(\mathbf{y}) - 2\sqrt{A(\mathbf{x})A(\mathbf{y})}C(\mathbf{x}, \mathbf{y}), \quad (69)$$

so when we know the law of overlap

$$C_t = \psi(C_{t-1}), \quad (70)$$

the law of distance is obtained in the form

$$D_t = \xi(D_{t-1}) \quad (71)$$

by using (69). For simplicity, we assume that $A(\mathbf{x})$ and $A(\mathbf{y})$ are equal to A^t . Then,

$$D_t = 2A^t(1 - C_t) \quad (72)$$

so we have the explicit form of $\xi(D)$ as

$$\xi(D_{t-1}) = 2A^t \left\{ 1 - \psi \left(1 - \frac{D_{t-1}}{2A^t} \right) \right\}. \quad (73)$$

Two random variables

$$u = \sum w_j x_j + b_j, \quad (74)$$

$$u' = \sum w_j y_j + b_j, \quad (75)$$

in which indices i and t are omitted for simplicity, are jointly Gaussian with mean 0 and their variances and covariances are written as

$$E[u^2] = E[u'^2] = \sigma_{A^t}^2, \quad (76)$$

$$E[uu'] = \sigma^2 A^t C(\mathbf{x}, \mathbf{y}) + \sigma_b^2 = \sigma_{A^t C}^2. \quad (77)$$

Then, we have the law of overlap from

$$C = \frac{1}{A^t} E[\varphi(u)\varphi(u')] \quad (78)$$

and by tedious calculations given in Appendix III,

$$C_t = \frac{1}{2\pi A^t} \cos^{-1} \left(-\frac{C_{t-1} A^t \sigma_t^2 + \sigma_b^2}{\sigma_{A^t}^2 \sqrt{1 + \sigma_{A^t}^2}} \right). \quad (79)$$

This gives the law of distance $\xi(D)$. It satisfies

$$\xi(0) = 0 \quad (80)$$

and is a monotonically increasing function of D . When $\sigma_t^2 = \sigma^2$, we obtain

$$\xi'(0) = \bar{\chi}_1 \quad (81)$$

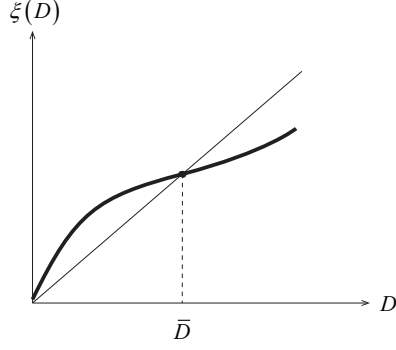


Figure 7: Law of distance

from the direct calculation or from the fact that the length of $d\mathbf{x}$ increases by the factor $\bar{\chi}_1$. Hence when $\bar{\chi}_1 < 1$, the distance converges to 0, so information processing is poor. When $\bar{\chi}_1 > 1$, the dynamics of distance (71) has a solution other than the 0 specified in equation (80),

$$\bar{D} = \xi(\bar{D}), \quad (82)$$

which is uniquely determined. See Fig. 7. The dynamics of distance converges to \bar{D} as $t \rightarrow \infty$, since the other equilibrium given in (80) is unstable. This implies that the distance between any two input signals \mathbf{x}_1 and \mathbf{x}_2 ($\mathbf{x}_1 \neq \mathbf{x}_2$) converges to \bar{D} as t goes to infinity, provided n_t are sufficiently large.

However, this is problematic, because X is an n -dimensional continuum. The neural transformation specified in equations (5) and (6) is continuous, so it is impossible that the distances of all pairs of two input signals become \bar{D} . A set Z of points in which any two points have the same distance \bar{D} consists of at most $N + 1$ points in an N -dimensional space. Therefore, it is impossible that X is mapped on Z by a continuous transformation. There exist frustrations between the distance and continuity, caused by the finiteness of n_t .

Let ξ^{*t} be the t times concatenation of the distance law:

$$\xi^{*t}(D) = \xi \{ \xi \cdots \{ \xi(D) \} \cdots \}. \quad (83)$$

It converges to the step function

$$\lim_{t \rightarrow \infty} \xi^{*t}(D) = \begin{cases} \bar{D}, & D > 0, \\ 0, & \text{otherwise.} \end{cases} \quad (84)$$

as t goes to infinity, where we assume $n \rightarrow \infty$. We consider a straight line

$$\mathbf{x}(s) = s\mathbf{x} \tag{85}$$

in X as a simple example and let

$$D(s) = D[\mathbf{x}(0), \mathbf{x}(s)], \tag{86}$$

which is the squared distance from the origin $\mathbf{x}(s) = 0$ to $\mathbf{x}(s)$. Then, the distance between two points after the t -th layer is given by

$$D^t(s) = \xi^{*t} \{D(s)\}. \tag{87}$$

When we consider the distance between $\mathbf{x}(s_1)$ and $\mathbf{x}(s_2)$, the distance after the transformation is given by

$$D[\tilde{\mathbf{x}}^t(s_1), \tilde{\mathbf{x}}^t(s_2)] = \xi^{*t}(s_2 - s_1). \tag{88}$$

From (84), we see that the curve $\tilde{\mathbf{x}}^t(s)$ has the fractal-like structure since we have $\xi^{*t}(\alpha s) = \xi^{*t}(s)$ for any α when t is large. There exist adversarial examples in a deep network. They are due to the fractal nature of the transformation.

The convergence of distance to \bar{D} is derived in the situation when $n \rightarrow \infty$ and then $t \rightarrow \infty$. It is known that

$$\lim_{t \rightarrow \infty} \lim_{n \rightarrow \infty} \xi^{*t}(D) = \lim_{n \rightarrow \infty} \lim_{t \rightarrow \infty} \xi^{*t}(D) \tag{89}$$

does not necessarily holds (see Amari, Yoshida & Kanatani, 1977, for the case of random recurrent networks). In reality, both n and t are finite. When n is finite, $\xi(D)$ suffers from random fluctuations, so (84) does not hold exactly. Hence the image of a curve $\mathbf{x}(s)$ is still a continuous curve, and the distance between $\mathbf{x}(s)$ and $\mathbf{x}(s')$, $s \neq s'$, is not exactly to \bar{D} . It is outside of the scope of the present papaer but is interesting to study how $D(\mathbf{x}(0), \mathbf{x}(s))$ behaves for large but finite n as t increases. The non-uniform convergence with respect to n and t is also seen in (66).

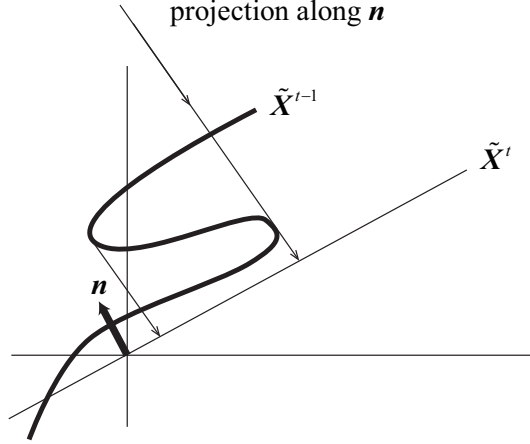


Figure 8: Dimension reduction and tearing of \tilde{X}^{t-1}

7 Collapse of manifolds when $n_t < n_{t-1}$

We have discussed the case with $n_t \geq n_{t-1}$, where the dimension numbers are non-decreasing. When $n_t < n_{t-1}$, dimension reduction takes place and the situation is completely different. In this case, there exists the null space of weight matrix $\mathbf{W}^t = (w_{ij}^t)$,

$$N = \{ \mathbf{x} \mid \mathbf{W}^t \mathbf{x} = 0 \}. \quad (90)$$

In other words, for any \mathbf{x} and $\mathbf{n} \in N$,

$$\mathbf{W} \mathbf{x} = \mathbf{W} (\mathbf{x} + \mathbf{n}). \quad (91)$$

This means that the null directions are collapsed by multiplication by \mathbf{W}^t .

The image \tilde{X}^{t-1} is a highly curved submanifold in X^{t-1} , so this dimension reduction tears \tilde{X}^{t-1} and many points in \tilde{X}^{t-1} are mapped to a point in X^t (see Figure 8). Then, nonlinear φ is applied. The activity, metric and curvature develops in the same way after the dimension reduction. How is the structure of \tilde{X}^t after dimension reduction is an interesting problem to be studied further.

8 Conclusions

Using the statistical neurodynamics of a multilayer perceptron of random connections, we have studied how the signal space geometry, metric, curvature, and distance between signals develop

as signals are processed in deep networks. The present asymptotic theory assumes that the number n_t of neuros in each layer is *sufficiently* large. We then found that the metric is conformally mapped from layer to layer, where the scale factor χ_1 plays a fundamental role in this mapping. When $\chi_t^* \approx 1$, the dynamics of $\tilde{\mathbf{x}}^t$ is chaotic and rich information processing takes place (Yang and Schonholtz, 2017). The curvature tensor and scalar curvature are obtained explicitly, showing that the curvature diverges to infinity when $\chi_t^* = 1$ provided n is finite. That is, creations of new curvatures are of order $1/n$, infinitesimally small, but are accumulated to infinity. This implies that the finite n effect is important. The metric $g_{\kappa\lambda}^t$ also fluctuates from $\chi_t^* \delta_{\kappa\lambda}$ and accumulates, when n is finite, which is important for accumulation of curvature. How the distance between two input signals develops is also shown.

Our results hold in the limit of $t \rightarrow \infty$ and $n \rightarrow \infty$, but in reality t and n are finite. So we need to study the effect of finiteness, which resolves apparently embarrassing results of the present theory. We need to study the finiteness effect carefully to resolve the contradiction. We have mostly focused on the case of $n_t \geq n_{t-1}$. However, information reduction takes place when $n_t < n_{t-1}$. We need to study this case in details in future work.

Appendix I: Useful formulas

The explicit forms of the fundamental functions $\chi_p(A)$ are obtained from the following formulas, where φ is the error function.

1)

$$\int_{-\infty}^{\infty} \varphi(au)\varphi(bu)Du = \frac{1}{2\pi} \cos^{-1} \left(\frac{-ab}{\sqrt{1+a^2}\sqrt{1+b^2}} \right), \quad (92)$$

2)

$$\int_{-\infty}^{\infty} \{\varphi'(au)\}^2 Du = \frac{1}{2\pi} \frac{a^2}{\sqrt{1+2a^2}}, \quad (93)$$

3)

$$\int_{-\infty}^{\infty} \{\varphi''(au)\}^2 Du = \frac{1}{2\pi} \left(\frac{a^2}{\sqrt{1+2a^2}} \right)^3. \quad (94)$$

By putting $a = b = \sigma_A$ in 1), we have

$$\chi_0(A) = \frac{1}{2\pi} \cos^{-1} \left\{ \frac{1}{1 + \sigma_b^2 + \sigma^2 A} - 1 \right\}. \quad (95)$$

By putting $a = \sigma_A$ in 2) and 3), we have

$$\chi_1(A) = \frac{\sigma^2}{2\pi} \frac{\sigma_b^2 + \sigma^2 A}{\sqrt{1 + 2(\sigma_b^2 + \sigma^2 A)}}, \quad (96)$$

$$\chi_2(A) = \frac{\sigma^4}{2\pi} \left(\frac{\sigma_b^2 + \sigma^2 A}{\sqrt{1 + 2(\sigma_b^2 + \sigma^2 A)}} \right)^3. \quad (97)$$

Equations (93) and (94) are easy to prove, because φ' is standard Gaussian. We prove 1).

We have

$$\int_{-\infty}^{\infty} \varphi(au)\varphi(bu)Du = \frac{1}{(\sqrt{2\pi})^3} \int_{-\infty}^{\infty} du e^{-\frac{u^2}{2}} \int_{-\infty}^{au} e^{-\frac{v^2}{2}} dv \int_{-\infty}^{bu} e^{-\frac{w^2}{2}} dw \quad (98)$$

$$= \frac{1}{(\sqrt{2\pi})^3} \int_R \exp \left\{ -\frac{u^2 + v^2 + w^2}{2} \right\} dudvdw, \quad (99)$$

where R is the region

$$R = \{(u, v, w) \in S_1 \cap S_2\}, \quad (100)$$

$$S_1 : v \leq au, \quad (101)$$

$$S_2 : w \leq bu. \quad (102)$$

S_1 and S_2 are the regions under the two planes $v = au$ and $w = bu$, both passing through the origin. The normal vectors of the two surfaces are

$$\mathbf{n}_1 = \left(\frac{a}{\sqrt{1+a^2}}, \frac{-1}{\sqrt{1+a^2}}, 0 \right), \quad \mathbf{n}_2 = \left(\frac{b}{\sqrt{1+b^2}}, 0, \frac{-1}{\sqrt{1+b^2}} \right). \quad (103)$$

The angle between S_1 and S_2 is $\theta = \pi - \cos^{-1}(\mathbf{n}_1 \cdot \mathbf{n}_2) = \cos^{-1}(-\mathbf{n}_1 \cdot \mathbf{n}_2)$. Hence, we have

$$1) = \frac{1}{2\pi} \cos^{-1} \frac{-ab}{\sqrt{1+a^2}\sqrt{1+b^2}}. \quad (104)$$

By putting $a = \sigma_A$,

$$\chi_0(A) = \frac{1}{2\pi} \cos^{-1} \frac{-(\sigma_A^2 + \sigma_b^2)}{1 + \sigma_A^2 + \sigma_b^2}. \quad (105)$$

This is monotonically increasing in $0 \leq A \leq 1$.

Appendix II

Split Lemma When w_1, \dots, w_n are independent random variables subject to $N(0, \sigma^2/n)$, the expectation of the product of two terms splits as

$$\mathbb{E}[f(\mathbf{w} \cdot \mathbf{x})k(\mathbf{w})] = \mathbb{E}[f(\mathbf{w} \cdot \mathbf{x})] \mathbb{E}[k(\mathbf{w})] \quad (106)$$

for arbitrary analytical functions f and $k(\mathbf{w}) = w_i w_j$ or $w_i w_j w_k w_l$, etc., when n is sufficiently large.

Proof. We prove the case of $k(\mathbf{w}) = w_i w_j$. For

$$u = \mathbf{w} \cdot \mathbf{x} = \sum w_i x_i \quad (107)$$

we define

$$\check{u}_{ij} = u - w_i x_i - w_j x_j. \quad (108)$$

Then, by Taylor expansion, we have

$$f(u) = f(\hat{u}_{ij}) + f'(\hat{u}_{ij})(w_i x_i + w_j x_j) \quad (109)$$

since w_i and w_j are small. Hence,

$$\mathbb{E}[f(u)k(\mathbf{w})] = \mathbb{E}[f(\hat{u}_{ij})] + \text{higher-order terms} \quad (110)$$

$$= \mathbb{E}[f(\hat{u}_{ij})] \mathbb{E}[k(\mathbf{w})] + \text{higher-order terms} \quad (111)$$

since \hat{u}_{ij} and $k(\mathbf{w})$ are independent. We again have

$$\mathbb{E}[f(\hat{u}_{ij})] = \mathbb{E}[f(u)] + \text{higher-order terms}. \quad (112)$$

□

The higher-order terms vanish as $n \rightarrow \infty$, so we have the lemma. The proof is similar when $k(\mathbf{w}) = w_i w_j w_k w_l$.

Appendix III: Law of distance

Let ε and ν be two independent standard Gaussian random variables subject to $N(0, 1)$. From equations (76) and (77), we have new representations of u and u' :

$$u = \sigma_A \varepsilon, \quad (113)$$

$$u' = \alpha \varepsilon + \beta \nu, \quad (114)$$

where

$$\alpha = \frac{\sigma_{AC}^2}{\sigma_A}, \quad \beta = \frac{\sqrt{\sigma_A^4 - \sigma_{AC}^4}}{\sigma_A}. \quad (115)$$

We see that

$$E [\varphi(u)\varphi(u')] = \frac{1}{(2\pi)^2} \int e^{-\frac{\varepsilon^2 + \nu^2}{2}} \int_{-\infty}^{\sigma_A \varepsilon} e^{-\frac{x^2}{2}} \int_{-\infty}^{\alpha \varepsilon + \beta \nu} e^{-\frac{y^2}{2}} dx dy d\varepsilon d\nu. \quad (116)$$

We first calculate the integration by y and ν , where we use

$$\int_{-\infty}^{\infty} \varphi(\alpha \varepsilon + \beta \nu) D\nu = \varphi\left(\frac{\alpha \varepsilon}{\sqrt{1 + \beta^2}}\right). \quad (117)$$

Then

$$E [\varphi(u)\varphi(u')] = E \left[\varphi(\sigma_A \varepsilon) \varphi\left(\frac{\alpha \varepsilon}{\sqrt{1 + \beta^2}}\right) \right]. \quad (118)$$

Since this is

$$\frac{1}{2\pi} \int \int_R \exp\left\{-\frac{y^2 + \nu^2}{2}\right\} dy d\nu \quad (119)$$

in the region

$$R : y \leq \alpha \varepsilon + \beta \nu, \quad (120)$$

calculating carefully, we finally have equation (79).

References

- [1] S. Amari, A Method of Statistical Neurodynamics. Kybernetik, Vol. 14, pp. 201–215, (Heft 4) April 1974.

- [2] S. Amari, H. Ando, T. Toyozumi and N. Masuda, State concentration exponent as a measure of quickness in Kauffman-type networks, *Physical Review E*, 87, 022814, 2013.
- [3] S. Amari, R. Karakida and M. Oizumi, Statistical neurodynamics of deep networks I, Geometry of signal spaces. arXiv, 2018.
- [4] S. Amari, K. Yoshida and K. Kanatani, A Mathematical Foundation for Statistical Neurodynamics, *SIAM J. Appl. Math.*, Vol. 33, pp. 95–126, 1977.
- [5] B. Poole, S. Lahiri, M. Raghu, J. Sohl-Dickstein and S. Ganguli, Exponential expressivity in deep neural network through transient chaos. In *Advances in Neural Information Processing (NIPS)*, 3360–3368, 2016.
- [6] L. I. Rozonoer, Random logical nets, I, II, III, *Avtomatika i Telemekhanika*, Nos. 5, 6, 7, 137–147, 99–109, 127–136, 1969.
- [7] S. S. Schoenholz, J. Gilmer, S. Ganguli and J Sohl-Dickstein, Deep information propagation. *ICLR’2017*, arXiv: 1611.01232, 2016.
- [8] H. Sompolinsky, A. Crisanti and H. J. Sommers, Chaos in random neural networks. *Physical Review Letters*, Vol. 61, pp. 259–262, 1988.
- [9] T. Toyozumi and H. Huang, Structure of attractors in randomly connected networks. *Physical Review*, E91, 032802, 2015.
- [10] G. Yang, S. Schoenholz, Mean field residual networks: On the edge of chaos. *Proc. NIPS*, 2865–2873, 2017.